

Propeller states in locally supercritical ULXs

M. Middleton,¹★ A. Gúrpide¹ and D. J. Walton²

¹*School of Physics & Astronomy, University of Southampton, Southampton, Southampton SO17 1BJ, UK*

²*Centre for Astrophysics Research, University of Hertfordshire, College Lane, Hatfield AL10 9AB, UK*

Accepted 2022 November 15. Received 2022 November 15; in original form 2022 August 26

ABSTRACT

An expected signature of the presence of neutron stars in the population of ultraluminous X-ray sources (ULXs) are large scale changes in X-ray luminosity, as systems reach spin equilibrium and a propeller state ensues. We explore the predicted luminosity changes when the disc is locally supercritical, finding that a significant parameter space in dipole field strength, and accretion rate (at large radius) can be accompanied by changes of less than an order of magnitude in luminosity. We discuss the spectral signature and locate three ULXs (IC 342 X-1, Cir ULX-5, and NGC 1313 X-1), which appear to show changes consistent with the super-Eddington systems entering a propeller state, and place rough constraints on the dipole field strength of NGC 1313 X-1 of $< 10^{10}$ G. This work implies that the most reliable means by which to search for putative propeller states will be to search for changes in hardness ratio and at high energies.

Key words: accretion, accretion discs – X-rays: binaries.

1 INTRODUCTION

The population of ultraluminous X-ray sources (ULXs) is undoubtedly a mixture of stellar-mass black holes and neutron stars, the vast majority of which are accreting at supercritical rates (the possibility remains that a small number of ULXs contain black holes of $\sim 100 M_{\odot}$ or more, accreting at or below their Eddington limit). Determining the nature of the intrinsic and observed population is important as it relates to the process of supercritical accretion, such as the role of geometrical beaming (e.g. King 2009; Middleton & King 2016, 2017; Wiktorowicz et al. 2019; Khan et al. 2022) and the strength of neutron star magnetic dipole fields (e.g. Mushtukov et al. 2015; King, Lasota & Kluźniak 2017; Middleton et al. 2019a; King & Lasota 2020; Brice et al. 2021; Kong et al. 2022), and is needed for simulations relying on populations of accreting binaries (e.g. Fragos et al. 2013; Kuranov, Postnov & Yungelson 2020; Kovelakas et al. 2022).

Locating neutron star ULXs (NS-ULXs hereafter) has relied on two approaches already widely used by the X-ray binary community: searches for pulsations and cyclotron resonance scattering features (CRSFs). The former have been detected in an increasing number of pulsing ULXs (PULXs, Bachetti et al. 2014; Israel et al. 2017a; Carpano et al. 2018; Sathyaprakash et al. 2019; Vasilopoulos et al. 2019; Rodríguez Castillo et al. 2020; Fuerst et al. 2021), whilst features resembling CRSFs have been located or inferred to be present in three ULXs to-date (Brightman et al. 2018; Walton et al. 2018c; Kong et al. 2022 although see also Koliopanos et al. 2019). It may be intrinsically very difficult to locate pulsations or CRSFs due to reprocessing in the cone of the wind or in the magnetospheric curtain if optically thick (Mushtukov et al. 2017, 2021) due to a lack of sufficient data quality, or simply due to the observing

band being too narrow to locate CRSFs. As a result, other ideas to separate the population have been proposed based on precession of a supercritical disc/wind (Middleton et al. 2018, 2019b; Khan et al. 2022) via their X-ray spectra (Koliopanos et al. 2017; Pintore et al. 2017; Walton et al. 2018b; Gúrpide et al. 2021a), or by associating ULXs undergoing large changes in X-ray flux with a propeller state. The latter approach assumes that a given NS-ULX is close to spin equilibrium (a reasonable assumption given the enormous spin-up rates, e.g. Bachetti et al. 2020) such that the co-rotation radius (R_{co}) moves inwards and approaches the magnetospheric radius (R_{m}). When this occurs accretion within R_{m} , i.e. through the magnetosphere and onto the neutron star itself may be completely or partially halted, with the abrupt change in luminosity permitting an estimate for the dipole magnetic field strength of the neutron star (e.g. Cui 1997; Tsygankov et al. 2016b). Attempts have been made to locate propeller states in ULXs by searching for large (over an order of magnitude) changes in X-ray brightness (e.g. Earnshaw, Roberts & Sathyaprakash 2018; Song et al. 2020, see also Vasilopoulos et al. 2021). However, such drops in brightness might also result from precession of the disc and wind (Pasham & Strohmayer 2013; Middleton et al. 2015a), or an increase in the scale height of obscuring material/narrowing of the wind-cone (Middleton et al. 2015a; Gúrpide et al. 2021b). Indeed, the continued spin-up of some PULXs during faint-states appears to confirm our line-of-sight to the central regions can indeed change (e.g. Vasilopoulos et al. 2019; Fuerst et al. 2021).

In this paper, we provide a description of propeller-induced luminosity changes based on super-Eddington accretion theory, and show that the dipole magnetic field strength of the neutron star can be constrained based on reasonable assumptions. We also provide a qualitative description of how the X-ray spectra may change under a propeller transition and tentatively identify such transitions for a handful of ULXs, constraining the dipole field strength in NGC 1313 X-1.

★ E-mail: m.j.middleton@soton.ac.uk

2 PROPELLER STATES IN LOCALLY SUPERCRITICAL ULXS

In the following, we will limit ourselves to the condition that the disc reaches the Eddington limit locally outside of R_m at the spherization radius given by $R_{\text{sph}} \approx \dot{m}_0 R_{\text{in}}$, where R_{in} is assumed to be the ISCO (whether reached by the disc or not, i.e. in the absence of truncating magnetic fields), and \dot{m}_0 is the accretion rate at very large radius in Eddington units; this is typically the mass transfer rate from the donor star unless some mass is lost at large radius due to thermal winds (Middleton et al. 2022). This condition (i.e. $R_{\text{sph}} > R_m$) which seems to be met in PULXs (e.g. King & Lasota 2020) requires the dipole field to not be extreme ($B > 10^{13-14}$ G), or that \dot{m}_0 is not too low. In such an accretion flow, the disc is assumed to follow standard theory (and knows nothing about the compact object at large radius, see Shakura & Sunyaev 1973), and launches winds to remain locally Eddington limited at all radii down to R_m . From R_m down to the neutron star surface (at R_{ns}), material is assumed to free-fall before forming a shock and dissipating the gravitational energy. It is highly likely that some of the material within the magnetospheric flow will be launched in a wind, however, this has not yet been explored in detail. We assume that the presence of winds (now directly observed in several ULXs: Middleton et al. 2014, 2015b; Pinto, Middleton & Fabian 2016; Walton et al. 2016; Pinto et al. 2017, 2020a; Kosec et al. 2018, 2021) acts to collimate radiation generated within R_{sph} . The collimation will be a function of radius (and \dot{m}_0 , cf King 2009; Jiang, Stone & Davis 2014, 2019), but here we will assume for simplicity that it can be parametrized at all radii within the wind-cone by $b = \Omega/4\pi$, where Ω is the solid opening angle of the wind (see King 2009). We also note that the observational impact on collimation is naturally system inclination-dependent (e.g. Dauser, Middleton & Wilms 2017; Middleton et al. 2021).

2.1 Propeller states without advection

We assume that binding energy liberated between R_m and the neutron star surface emerges either directly as pulsed emission, or via reprocessing in the magnetosphere (Mushtukov et al. 2017). The sum total luminosity of this radiative component is therefore limited to:

$$L_{\text{ns}} = GM_{\text{ns}} \dot{M}_m \left[\frac{1}{R_{\text{ns}}} - \frac{1}{R_m} \right], \quad (1)$$

where R_{ns} is assumed to be 10 km, and \dot{M}_m is the mass accretion rate at R_m (and where we are explicitly assuming no mass loss between R_m and the neutron star surface even though this might well occur in practice). Assuming the opening angle of the radiating surface (both magnetosphere and star) subtends a larger solid angle than the wind opening angle, it will be collimated by the wind-cone to yield an observed luminosity of:

$$L_{\text{ns,o}} = \frac{GM_{\text{ns}} \dot{M}_m}{b} \left[\frac{1}{R_{\text{ns}}} - \frac{1}{R_m} \right]. \quad (2)$$

We expect an intrinsic accretion luminosity from the disc between R_m and R_{sph} of:

$$L_{\text{disc}} = L_{\text{Edd}} \left[\ln \left(\frac{R_{\text{sph}}}{R_m} \right) + 1 \right]. \quad (3)$$

where the ‘+1’ refers to emission from the relatively thin disc beyond R_{sph} , which emits close to the Eddington limit (although flux from this region is likely to be intercepted and re-radiated from the photosphere of the wind; Poutanen et al. 2007). In practice regardless

of radial advection, the luminosity detected as radiation will be reduced by a factor $\xi = 1 - \epsilon_w$ (where ϵ_w is the fraction of the accretion luminosity used in driving the wind; Poutanen et al. 2007). The value of ϵ_w is as-yet unknown (values vary between 0.25 from simulations: Jiang et al. 2014 to close to unity from observations of the densest phases of the wind; Pinto et al. 2016). We assume that only the emission generated within R_{sph} is collimated, such that the observed luminosity from this region is then given by:

$$L_{\text{disc,o}} = L_{\text{Edd}} \left[\frac{\xi}{b} \ln \left(\frac{R_{\text{sph}}}{R_m} \right) + 1 \right]. \quad (4)$$

Before the propeller state is entered and accretion onto the neutron star is assumed to switch off, we expect to observe $L_{\text{ns,o}} + L_{\text{disc,o}}$, whilst in a propeller state we should see only the emission from outside of R_m , i.e. $L_{\text{disc,o}}$. This implies that for accretion rates, where $\frac{\xi}{b} \ln \left(\frac{R_{\text{sph}}}{R_m} \right) \gg 1$, and assuming that b is similar for both components (supercritical disc and accretion column/magnetosphere), the beaming factor can be eliminated to leave:

$$\frac{\Delta L}{L_{\text{disc,o}}} = \frac{L_{\text{ns,o}}}{L_{\text{disc,o}}} \approx \frac{GM_{\text{NS}} \dot{M}_m}{L_{\text{Edd}} \xi \ln \left(\frac{R_{\text{sph}}}{R_m} \right)} \left[\frac{1}{R_{\text{NS}}} - \frac{1}{R_m} \right], \quad (5)$$

which in the limit of high dipole field strength (such that $R_m \gg R_{\text{ns}}$), using canonical values and assuming the standard linear scaling of accretion rate with radius (i.e. neglecting advection: $\dot{m} = \dot{m}_0 R/R_{\text{sph}}$ Shakura & Sunyaev 1973), can simplify to:

$$\frac{\Delta L}{L_{\text{disc,o}}} \approx \frac{0.208 \dot{m}_0 R_m}{\eta \xi R_{\text{sph}}} \left[\ln \left(\frac{R_{\text{sph}}}{R_m} \right) \right]^{-1}, \quad (6)$$

where η is the radiative efficiency for accretion at the inner edge of the accretion disc (assumed to be ~ 0.08). In the above, R_m can be assumed to be related to the dipole field strength (B) via standard relations modified for super-Eddington accretion flows (i.e. once again assuming a simple linear radial dependence for the accretion rate: Shakura & Sunyaev 1973). Assuming a canonical neutron star mass of $1.4M_{\odot}$ gives:

$$R_m \approx 4.2 \times 10^7 B_{12}^{4/9} [\text{cm}], \quad (7)$$

where B_{12} is the dipole magnetic field strength in units of 10^{12} G (and the magnetic dipole moment, $\mu = BR_{\text{ns}}^3$). It is clear from equations 5–7 that for $R_m < R_{\text{sph}}$, the change in luminosity during a transition to a propeller state relative to the luminosity during a propeller state is a function of \dot{m}_0 and B (and an assumed value for ξ). Using equations 5 & 7 (which allows us to cover the full range of dipole field strengths), we plot the resulting values for $\Delta L/L_{\text{disc,o}}$ in Figs 1 and 2 for B between 10^9 – 10^{13} G, \dot{m}_0 between 10 and 1000, and assuming values for ϵ_w of 0.25 and 0.95, respectively. We note that we exclude those cases where R_m dips below the location of the ISCO (assumed to be $6R_g$), within which the nature of the coupling is unclear.

Fig. 1 (where $\epsilon_w = 0.25$) shows that whilst substantial changes in luminosity are certainly possible for low to moderate accretion rates and high-dipole field strengths, it is clear that a drop in total luminosity of less than a factor 10 can also occur for a wide range of dipole field strengths (between 10^9 and 10^{11} G coupled with a range in \dot{m}_0 between 10 and 1000). For those face-on and extremely bright sources, the source may well remain a very bright ULX even when in the propeller state. The same is true for Fig. 2 (where $\epsilon_w = 0.95$) but to a lesser degree; as expected, less energy escapes as radiation from the disc, and $\Delta L/L_{\text{disc,o}}$ is therefore larger for a given \dot{m}_0 and B .

As the mass of the compact object in this picture is assumed to be known within a small range, \dot{m}_0 can be estimated from the equation of

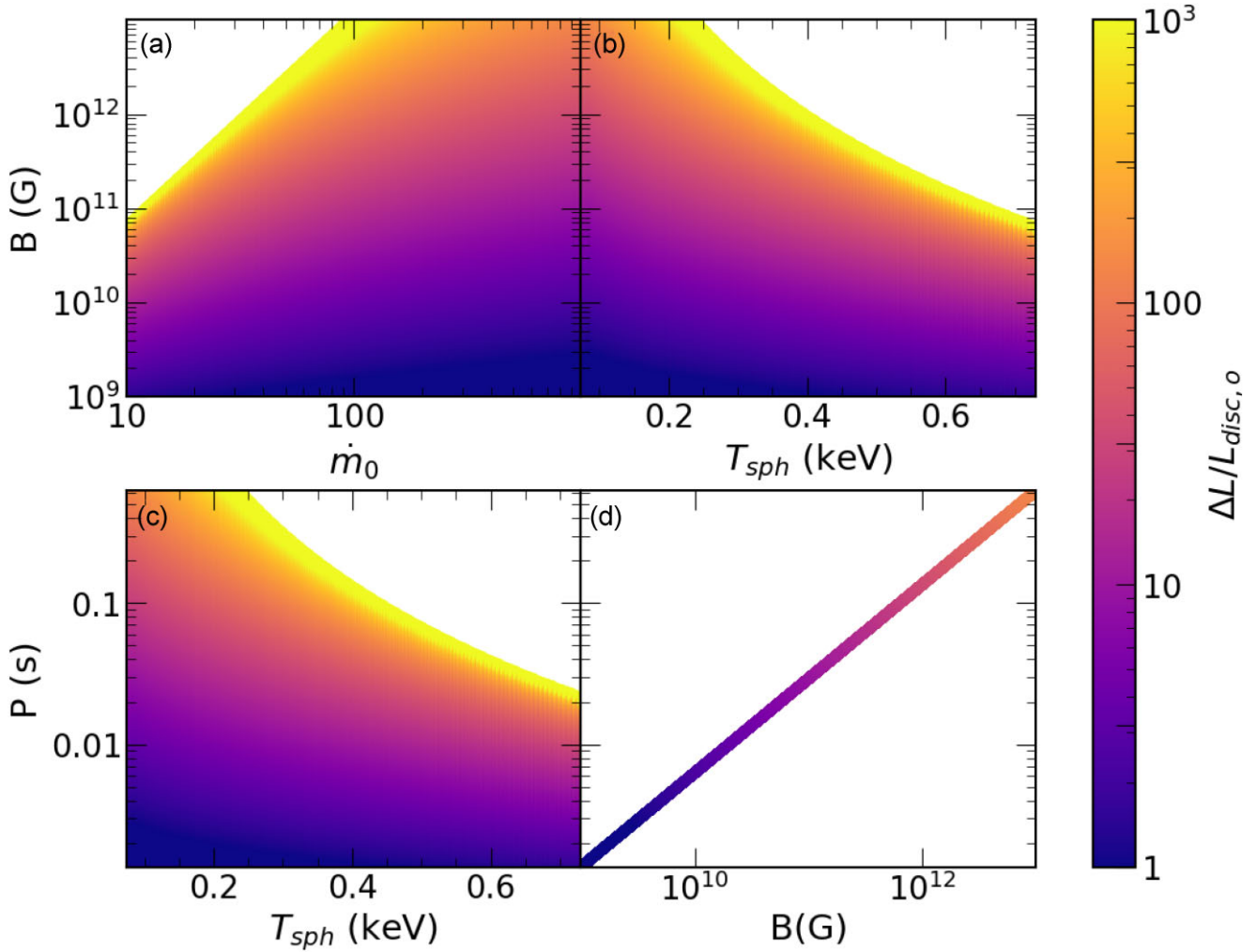


Figure 1. Plots showing the dependence of $\Delta L/L_{\text{disc},0}$ on the dipole magnetic field strength, B , and the accretion rate at large radius in Eddington units, \dot{m}_0 (Panel A). The latter may, alternatively, be parametrized by the temperature at the spherization radius, T_{sph} (Panel B), whilst the dipole magnetic field strength is related to the neutron star spin period at equilibrium (Panels C & D). These calculations have assumed no explicit advection, but a loss of energy to the wind parametrized by $\epsilon_{\text{wind}} = 0.25$.

Poutanen et al. 2007: $T_{\text{sph}} \approx 1.5 f_{\text{col}} m^{-1/4} \dot{m}_0^{-1/2}$ keV, where f_{col} is the colour temperature correction factor (for which we assume a value of 1.8). As a characteristic temperature can be easily obtained from soft X-ray spectra of ULXs (which will not be confused with emission from the magnetosphere when the field is only of moderate strength: Mushtukov et al. 2017, see section 3), in principle, this allows the dipole field strength to be estimated directly from the combination of X-ray spectra and relative change in luminosity (although see the Discussion for issues related to obtaining an accurate value for T_{sph}). The relative changes in the luminosity associated with the onset of a propeller state versus T_{sph} and B are also shown in Figs 1 and 2.

Given the requirement that R_m is equal to the co-rotation radius at the point where the propeller transition occurs, we are also able to predict the spin period of the neutron star (P_{ns}) through equating R_m to the co-rotation radius given by $R_{\text{co}} = (GM_{\text{ns}} P_{\text{ns}}^2 / 4\pi^2)^{1/3}$:

$$P_{\text{ns}} \approx 0.16 \frac{B_{12}^{2/3}}{\sqrt{m}} \text{ [s]}, \quad (8)$$

where m is the neutron star mass in units of M_{\odot} . The equivalent plots of B versus P_{ns} and T_{sph} versus P_{ns} are shown in Figs 1 and 2, respectively.

2.2 Propeller states with advection

The previous subsection assumed no explicit advection of matter and radiation within the disc, with only a fraction of the accretion power lost in driving in the wind (Poutanen et al. 2007). Whilst the true impact of advection on the cooling of the supercritical flow is still unclear (e.g. magnetic buoyancy may help radiation escape: Jiang et al. 2014), as discussed in Chashkina et al. (2019) including a radial advection term leads to a higher accretion rate at R_m , which increases the accretion rate onto the neutron star at which point the energy must be released.

Following Poutanen et al. (2007) and Middleton et al. (2019b), we include the effect of advection by setting the constant $a = \epsilon_w (0.83 - 0.25\epsilon_w)$, which enters the radial profile of \dot{m} (noting that this differs to the simple profile assumed in the previous subsection; Poutanen et al. 2007), which we then solve numerically to obtain R_m (see Middleton et al. 2019b for details). The equivalent plots when including advection are shown in Figs 3 and 4 for values of ϵ_w of 0.25 and 0.95, respectively (noting that the formula for P_{ns} also now depends on the advective term). As expected, the result of advection is a decrease in brightness of the accretion disc (as energy is advected radially inwards), and a corresponding increase

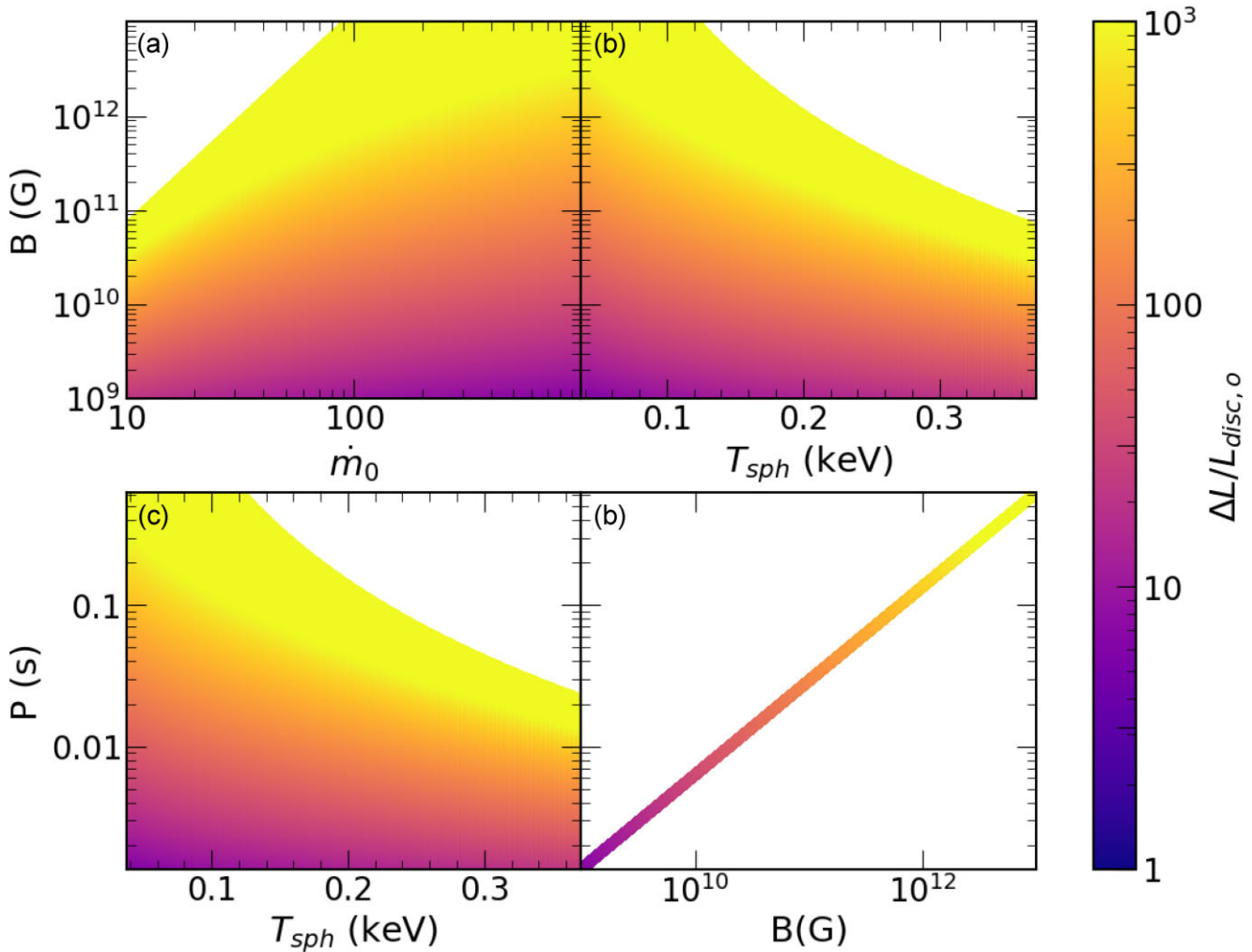


Figure 2. As per Fig. 1 but with $\epsilon_{\text{wind}} = 0.95$.

in brightness of the regions within R_m (assuming the neutron star can actually accommodate such rates of infall, otherwise mass loss must ensue). Together, this results in an increase in $\Delta L/L_{\text{disc},o}$ compared to the case without explicit advection (cf Figs 1 and 2).

3 SEARCHING FOR POSSIBLE PROPELLER STATES IN ULXS

It is crucial to note that in order to determine the dipole field strength using the above formulae, we require a bandpass where the accretion column (reprocessed or direct) can be seen to switch off. As noted by Brightman et al. (2016) and Walton et al. (2018a), the pulsed component can be directly and unambiguously identified in PULXs and dominates above a few keV. This component may be present in other ULXs, even where pulsations have not been observed (Pintore et al. 2017; Walton et al. 2018b). A natural corollary is that a propeller state will be associated with this high-energy component – noted to remain stable across many observations in some ULXs (e.g. Walton et al. 2017, 2020; Gúrpede et al. 2021a) – dropping away. In addition to the accretion column, we would also expect any emission from within R_m , i.e. from the accretion curtain to also fall away, however, importantly, the entire broad-band flux, especially at low energies does not need to fall to zero. To confirm the range of temperatures, we would expect from the accretion curtain, we employ the formulae

of Mushtukov et al. (2017) assuming the curtain is optically thick throughout and able to efficiently reprocess all of the emission from the fan-beam within (noting that complete reprocessing is a limiting assumption). The emergent temperature is altered by some colour temperature correction factor (f_{col} which we again set to a value of 1.8), and is given by the formula:

$$T_{\text{cur}} = k f_{\text{col}} \left(\frac{L_{\text{ns}}}{4\pi R_m^2 \sigma} \right)^{1/4} \text{ [keV]}, \quad (9)$$

where k is the Boltzmann constant, σ is the Stefan–Boltzmann constant, and L_{ns} is the intrinsic luminosity generated from free-fall onto the neutron star (i.e. $bL_{\text{ns},o}$). For the ranges of dipole field strength and \dot{m}_0 , we explore here, we plot the corresponding value of T_{cur} in Fig. 5. It is apparent that the peak of the emission ($\sim 3 T_{\text{cur}}$) will be above 2–3 keV in all cases we are considering. This component is therefore unlikely to be readily confused with the soft component seen in most ULXs (e.g. Middleton et al. 2015a) unless only a very small fraction of the fan beam luminosity is reprocessed (which would tend to conflict with the inferred luminosity of the soft component).

Based on the above argument, ULXs where $R_m < R_{\text{sph}}$ entering the propeller regime should remain relatively bright in the soft band, while the emission above ~ 2 keV should drop significantly. This scenario may be able to explain the unusual spectral states found in

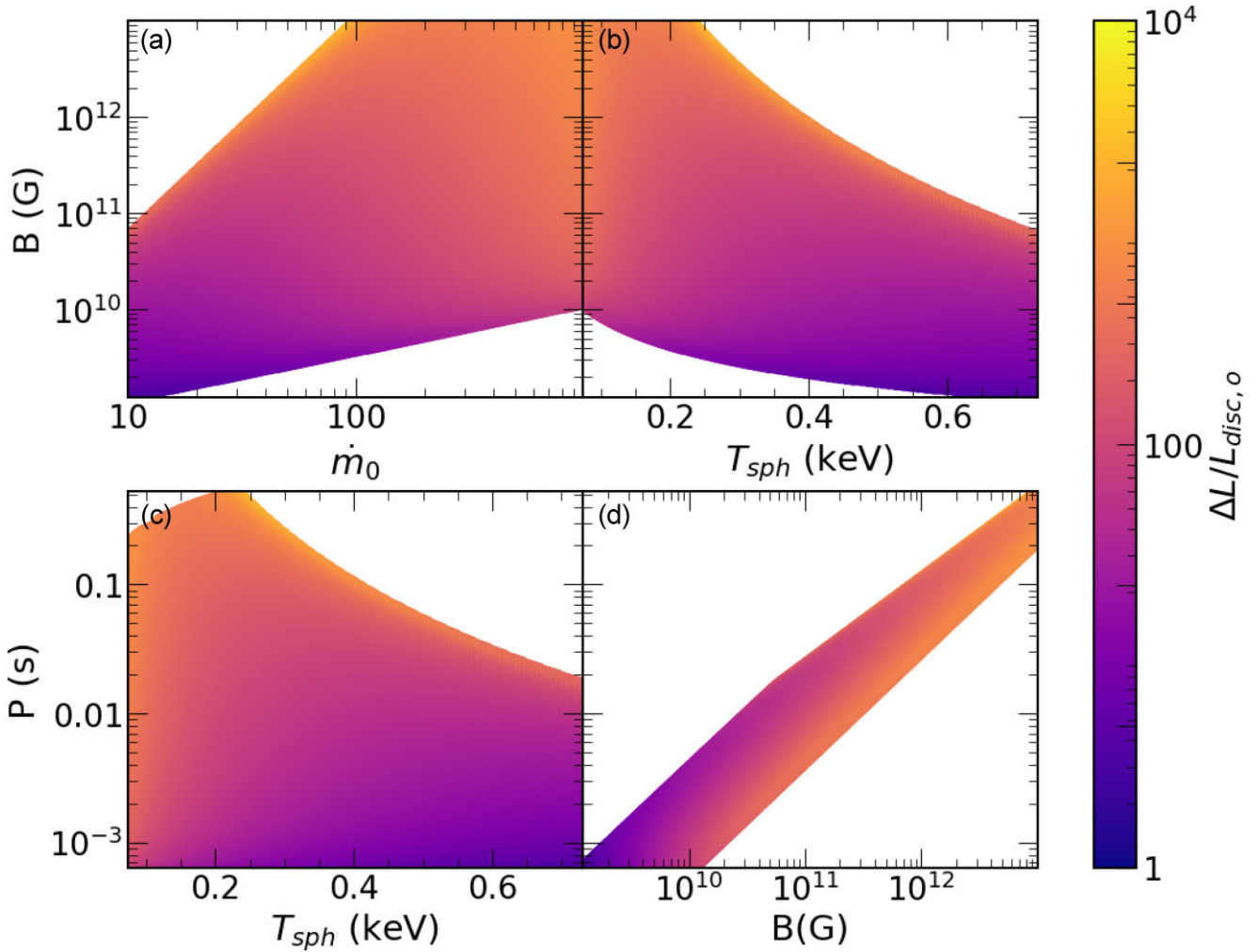


Figure 3. As per Fig. 1 with explicit advection (see Poutanen et al. 2007; Middleton et al. 2019b), and a loss of energy to wind parametrized by $\epsilon_{\text{wind}} = 0.25$.

IC 342 X-1 (Marlowe et al. 2014; Gúrpile et al. 2021a), where it appears that, between two observations separated in time, the unabsorbed luminosity in the soft band has remained stable but the hard band luminosity has dropped by a factor ~ 2 (Gúrpile et al. 2021a). Interestingly, this source has been proposed as a good NS-ULX candidate based on its hard X-ray spectrum (Pintore et al. 2017; Gúrpile et al. 2021a). Gúrpile et al. (2021a) noted similar transitions in NGC 1313 X-1 (see also Middleton et al. 2015a) and Circinus ULX 5, where the hard flux also dropped by a factor $\sim 2-3$, with stable flux in the soft band. We revisit these spectral changes and using the above formulae attempt to provide initial estimates for the dipole magnetic field strength under the assumption that these spectral changes are caused by a transition to the propeller regime. More specifically, we used *XMM-Newton* observations 0206890101, 0205230601, 0111240101 for the high-state spectra of IC 342 X-1, NGC 1313 X-1, and Circinus ULX 5, respectively, and *Chandra* observation 13686 and *XMM-Newton* observations 0205230401, 0792382701 for the suspected propeller states of IC 342 X-1, NGC 1313 X-1, and Circinus ULX 5.

The spectral products were taken from Gúrpile et al. (2021a) and modelled in *XSPEC* version 12.12.1 using `tbabs@diskbb + nthcomp` following Middleton et al. (2015a), and using abundances and cross sections from Wilms, Allen & McCray 2000,

Verner et al. 1993 and Verner and Yakovlev 1995. Given the above picture, we require the soft component to be fairly stable between observations, whereas the hard component should have dropped in the propeller state. Therefore, we simultaneously fitted the two sets of spectra for each ULX, tying the luminosity of the `diskbb` and removing the `nthcomp` (the emission within R_m) from the propeller state. The absorption column is also tied between observations, with the lower limit set at the respective line-of-sight column densities. We computed de-absorbed model fluxes between 0.01 and 50 keV (to capture the total flux), using the pseudo-model `CFLUX` for each of the model components (the `diskbb` and the `nthcomp`). It is important to note that the thermal tail of the `nthcomp` component may lead to a slight underestimate of the total flux above 10 keV (where the true emission is flatter than Wien, see e.g. Walton et al. 2020). For the sake of brevity, we present only the most relevant spectral parameters in Table 1, and direct the reader to the literature for a more complete picture of the spectral analysis of these sources (e.g. Marlowe et al. 2014; Middleton et al. 2015a; Gúrpile et al. 2021a). The spectral transitions between the high and putative propeller states and the best-fitting models are shown in Fig. 6.

Using the values in Table 1 and the formulae in this paper, we can attempt to place some constraints on the strength of the dipole field in the three ULXs assuming they contain neutron stars.

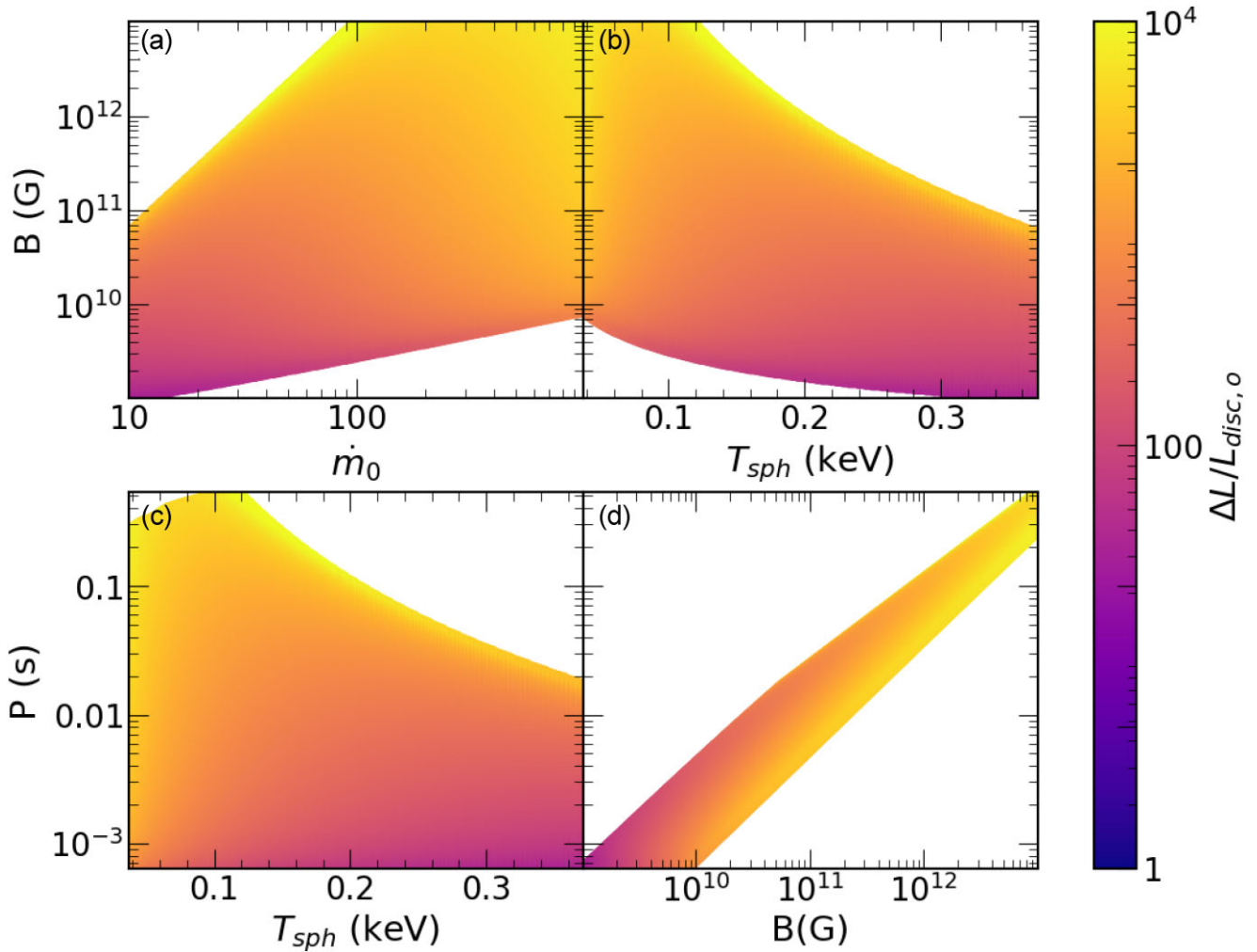


Figure 4. As per Fig. 3 but with $\epsilon_{wind} = 0.95$.

Notably, all luminosities during the putative propeller state are above the Eddington luminosity for a neutron star requiring $R_{sph} > R_m$, which matches the regime where our formulae should be reasonable approximations.

From Figs 1–4, it is apparent that the dominant uncertainty on any estimate for the dipole field strength via a propeller state is the role of advection and the value of ϵ_w . For a given $\Delta L/L_{disc,0}$, the case with low ϵ_w and no advection appears to place the most generous upper limit on the dipole field strength given a measurement of T_{sph} . However, it is important to note that T_{sph} is currently estimated from a highly simplified model (DISKBB) which will be a poor description of the anisotropic supercritical disc, and only return the highest temperature, not necessarily that from R_{sph} (instead, the temperature could correspond to emission from smaller radii); addressing this issue is beyond the scope of this paper, but work is in progress to provide the community with more physically appropriate models. In the cases of IC 342 X-1 and Cir ULX-5, the implied column density is very high which may be further complicating our modelling of the soft emission. We therefore focus only on NGC 1313 X-1; given the values in Table 1 and the limits imposed by the case of no advection and low ϵ_w , we would estimate an upper limit of $B < 10^{10}$ G unless the temperature estimated for T_{sph} is incorrect by over an order of magnitude.

4 DISCUSSION AND CONCLUSIONS

Searching for propeller states in ULXs is a promising means by which to locate neutron star accretors (e.g. Earnshaw et al. 2019; Song et al. 2020). In this paper, we have utilized the formulae for supercritical discs with mass loss and advection to explore the signatures of propeller states. In the case where radial advection is weak (such that only the local accretion luminosity escapes from within R_m and a simple linear scaling of accretion rate with radius is assumed: Shakura & Sunyaev 1973), and a low fraction of the accretion power is used to drive the wind, propeller states with predicted drops in total luminosity of less than an order of magnitude exist across a substantial area of parameter space (in \dot{m}_0 and dipole field strength). Notably, even those large changes which accompany large dipole field strengths may still appear as (soft) ULXs when in a propeller state (cf Erkut et al. 2019). Including radial advection (where the mass accretion rate now scales in a more complex manner: Poutanen et al. 2007) results in far larger changes in luminosity for a given dipole field strength, as relatively more accretion energy escapes at the neutron star surface (although it is likely that excess energy will be used to drive material from the magnetosphere). By combining the results with and without advection, it is clear that locating a source unambiguously entering a propeller state should allow constraints to be placed on the strength of the dipole magnetic field.

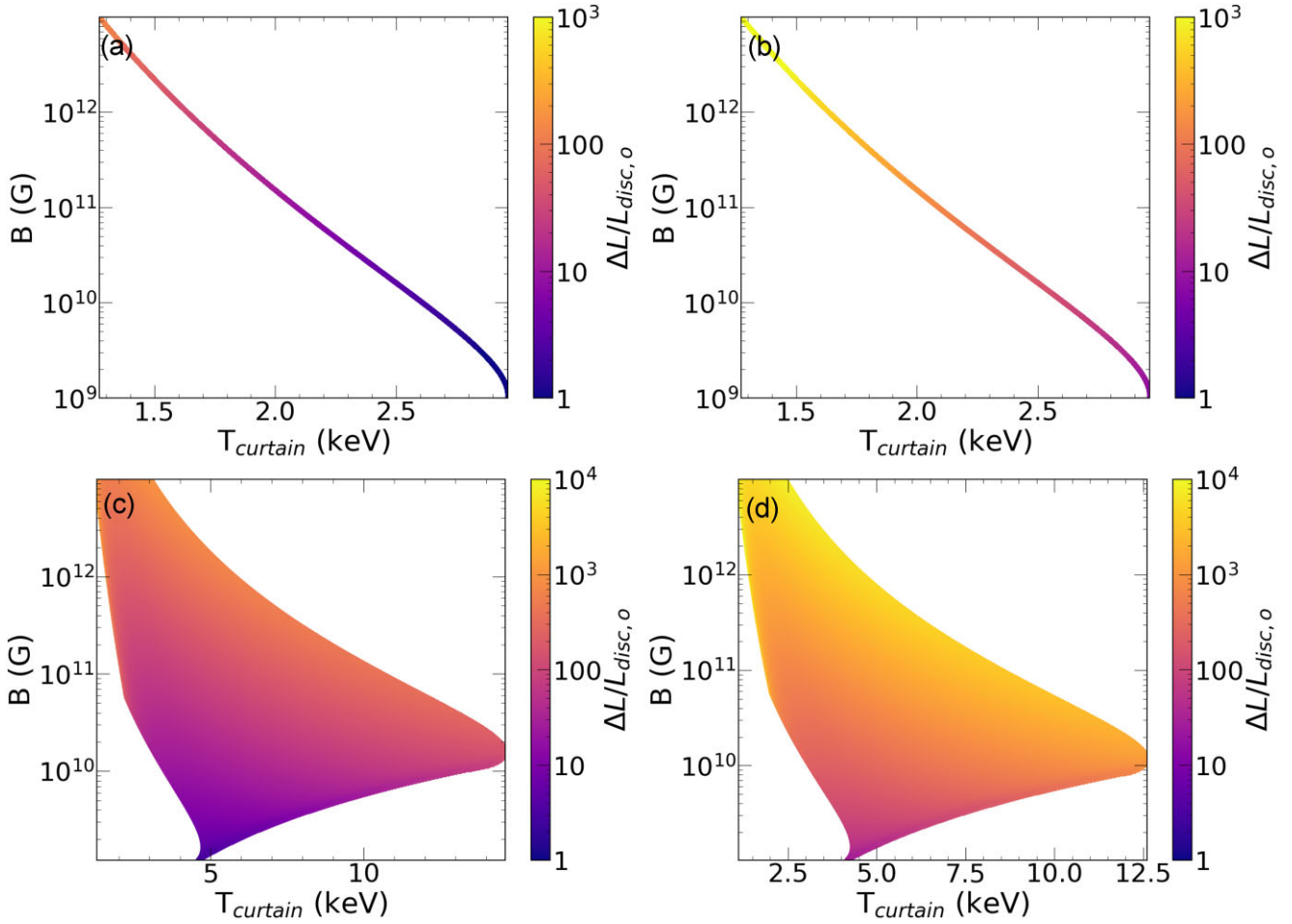


Figure 5. Plots showing the dependence of $\Delta L/L_{\text{disc},o}$ on the dipole magnetic field strength, B , and the temperature of the accretion curtain (see Mushtukov et al. 2017). Panels A & B assume no advection with $\epsilon_{\text{wind}} = 0.25$ and 0.95 , respectively, whilst Panels C & D have assumed explicit advection (see Poutanen et al. 2007; Middleton et al. 2019b) with $\epsilon_{\text{wind}} = 0.25$ and 0.95 , respectively.

Table 1. Best-fit parameters for the putative propeller transitions. The model used for the high state was `tbabs@ (diskbb + nthcomp)`, while for the propeller state the same model was used but without the `nthcomp`. $L_{\text{disc},o}$ and $L_{\text{ns},o}$ refer to the unabsorbed 0.01–50 keV luminosities of the `diskbb` and `nthcomp` model components, respectively. Uncertainties are at the 1σ confidence level. Distances adopted for the luminosity calculations are: 3.39, 4.25, and 4.21 Mpc for IC 342 X–1, NGC 1313 X–1, and Circinus ULX5, respectively (Tully, Courtois & Sorce 2016).

| Source | State | N_{H} $\times 10^{20} \text{ cm}^{-2}$ | kT_{soft} keV | $L_{\text{disc},o}$ $\times 10^{39} \text{ erg s}^{-1}$ | $L_{\text{ns},o}$ $\times 10^{39} \text{ erg s}^{-1}$ | $\Delta L/L_{\text{disc},o}$ | χ^2/dof |
|---------------|-----------|--|---------------------------|--|--|------------------------------|---------------------|
| IC 342 X-1 | High | 0.80 ± 0.02 | 0.87 ± 0.02 | $5.9^{+0.2}_{-0.1}$ | 5.1 ± 0.2 | 0.86 ± 0.04 | 476/417 |
| | Propeller | – | – | – | – | – | – |
| NGC 1313 X-1 | High | 0.15 ± 0.01 | 0.57 ± 0.01 | $4.7^{+0.09}_{-0.07}$ | 4.2 ± 0.2 | $0.90^{+0.05}_{-0.04}$ | 717/390 |
| | Propeller | – | – | – | – | – | – |
| Circinus ULX5 | High | 0.63 ± 0.01 | $1.13^{+0.01}_{-0.02}$ | 5.15 ± 0.05 | 8^{+8}_{-3} | $1.5^{+1.6}_{-0.6}$ | 518/374 |
| | Propeller | – | – | – | – | – | – |

Tsygankov et al. (2016a) explored the dipole field strength implied by the factor ~ 40 change in luminosity of M82 X-2 under the assumption of a propeller state where the disc beyond R_m is not locally supercritical, finding the field to be $\sim 10^{14}$ G. Using our formulae, we would only obtain solutions where the spin period was faster than observed, implying that our assumptions have broken down (i.e. that $R_m > R_{\text{sph}}$) or that the change is not consistent with a propeller transition. Indeed, we now believe the changes in M82 X-2’s flux to be driven by an entirely different effect (due to their

periodic nature seeming to match other ULX superorbital periods Brightman et al. 2019a).

A key signature of a propeller state in those ULXs, where $R_m < R_{\text{sph}}$ is a drop at hard X-ray energies above 2 keV (see Fig. 5) as the column and curtain (Mushtukov et al. 2017) switch off, whilst the soft X-ray emission should remain essentially unchanged across the transition. Similar spectral changes might result from precession of the disc and wind (e.g. Middleton et al. 2015a, 2019b), however, in those cases, we would expect some changes at soft energies as the beaming pattern

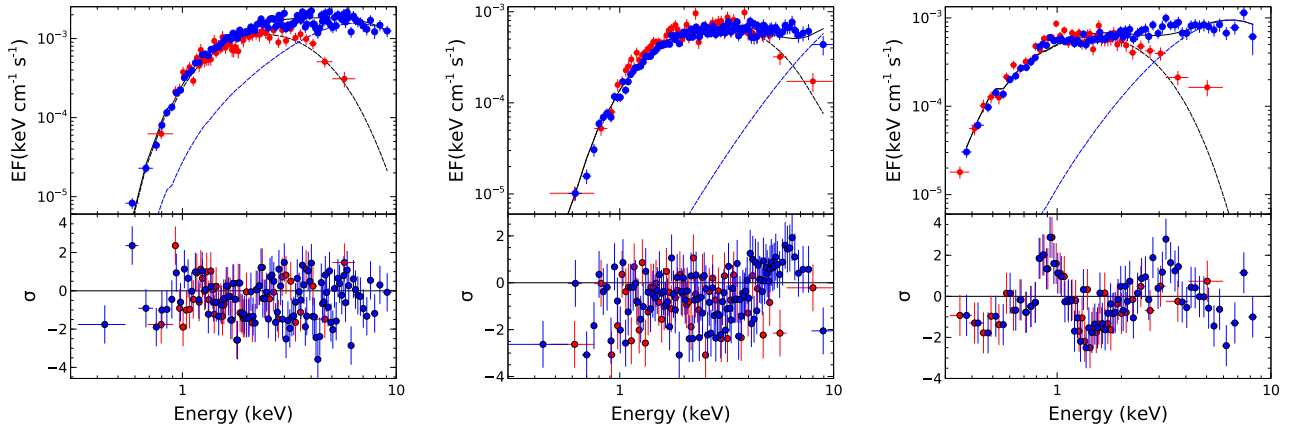


Figure 6. Spectral transitions tentatively attributed to propeller transitions. From left to right, the panels show IC 324 X-1, Cir ULX-5, and NGC 1313 X-1. All panels show *XMM-Newton* EPIC PN data, except for the low state of IC 324 X-1 and the high state of Cir ULX-5, where *Chandra*-ACIS and EPIC MOS1 data are shown instead. The high state and low (propeller) states are coloured in blue and red, respectively. The `diskbb` component (which is tied between states) is shown by a black dashed line, the `ntbcomp` by a dashed blue line, and the total model by a solid black line. Data has been rebinned for the purpose of clarity.

has a radial dependence. This implies that searches which incorporate observations at high energies and hardness/flux ratios may be more efficient than simple searches for changes in luminosity (and will be better suited to locate the more subtle changes where the dipole field is weak). This line of reasoning provides additional evidence against major propeller-driven changes in M82 X-2, as the spectrum remains hard in the low-luminosity state (Brightman et al. 2019b). However, in the case of M82 X-2, true spin-down has already been observed (Bachetti et al. 2020) without a major change in luminosity from the ULX. Unless the dipole field is weak, this implies material is still being fed at a substantial rate onto the neutron star, and points to some natural complexity in how the field couples to the surrounding material. In such cases where the spectrum is unchanged, and therefore not the ideal picture described above where accretion is completely halted within R_m , the change in luminosity instead places a lower limit on the dipole field strength.

We have examined three ULXs where there appears to be spectral evidence in favour of the systems having entered a propeller state, IC 342 X-1, NGC 1313 X-1, and Circ ULX-5. All three ULXs show spectra where the hard component has fallen away (noting that this component in ULXs tends to have a similar shape at high energies: e.g. Walton et al. 2017) leaving only a soft component. We are able to match the soft component to other observations of the same ULX and obtain some estimate for $\Delta L/L_{\text{disc.o}}$. It is important to note that these observations are not contiguous (i.e. we do not catch a transition into propeller), and so it is quite possible that there could be small changes in inclination and/or \dot{m}_0 . Interestingly in the case of NGC 1313 X-1, the CCD residuals – now known to indicate the presence of a mass-loaded wind (Middleton et al. 2014, 2015b; Pinto et al. 2016; Walton et al. 2016; Kosec et al. 2021) – remain at a similar strength in both the high and propeller states, implying that winds of a similar strength are being driven even when emission from smaller radii is absent. The lack of change in CCD residual strength may well be an argument against precession producing this specific spectral change, as the strength of the atomic lines in NGC 1313 X-1 vary with spectral hardness as would be expected to accompany precession (Middleton et al. 2015b; Pinto et al. 2020b).

The key parameters we can extract from the X-ray spectrum are a characteristic temperature at soft energies, typically associated with the spherization radius, and the component luminosities in both states. In the cases of IC 342 X-1 and Circinus ULX-5, the soft

emission is harder to model due to the large absorption columns, and we obtain higher temperatures than the vast majority of ULXs (Middleton et al. 2015a). Although the spectrum is easier to reliably model in NGC 1313 X-1, we note that estimates of T_{sph} from applying available models is highly uncertain and the mismatch between phenomenological models, and the true anisotropy of supercritical discs is likely to produce overestimates for T_{sph} . Regardless, we infer that in the most constraining condition of no advection and limited loss of accretion power to the wind, the dipole field in NGC 1313 X-1 – should it harbour a neutron star – should be $<10^{10}$ G. Should this be correct, the corresponding neutron star rotation period should be very short (\sim ms) and would be heavily diluted due to the signal being scattered in the wind cone (Mushtukov et al. 2021). Such a weak dipole field strength is at odds with those measured for HMXBs in our own Galaxy (e.g. Bellm et al. 2014; Fürst et al. 2014) and even those other ULXs, where the field is estimated from the spin-up rate (e.g. Fürst et al. 2016; King et al. 2017; Carpano et al. 2018), but is consistent with the recent study of a ULX in M 101 (4XMM J140314.2+541806) by Urquhart et al. (2022), where the dipole field was estimated to be of a similar strength ($\sim 10^{10}$ G) based on a possible propellor state transition. Such relatively low-dipole fields could be consistent with the field being buried due to the high rates of accretion (e.g. Geppert & Urpin 1994), and may well be accompanied by stronger higher order fields (Israel et al. 2017b,c; Middleton et al. 2019a; Brice et al. 2021; Kong et al. 2022).

We should be observing true propeller states in the ULXs studied in this paper, we must consider the process driving R_{co} to approach R_m . Should the accretion rate be constant over time (noting that there are means by which to modulate this at large radius: Middleton et al. 2022), then the role of advection should be unchanged, and R_{co} can only move inwards as the neutron star extracts angular momentum from the disc and spins up (noting that the accretion torque asymptotes to zero as R_m approaches R_{co} – Dai & Li 2006 – demanding that some other process triggers the onset of the propellor state itself). This would imply that $R_{\text{co}} \approx R_m$ and we should not observe propeller transitions with any preference for spectral appearance, instead spectral changes would need to be driven by precession (Middleton et al. 2015a). Alternatively, should \dot{m}_0 be changing with time, the impact of advection should also change (e.g. Chashkina et al. 2019). In the model we have applied a larger \dot{m}_0

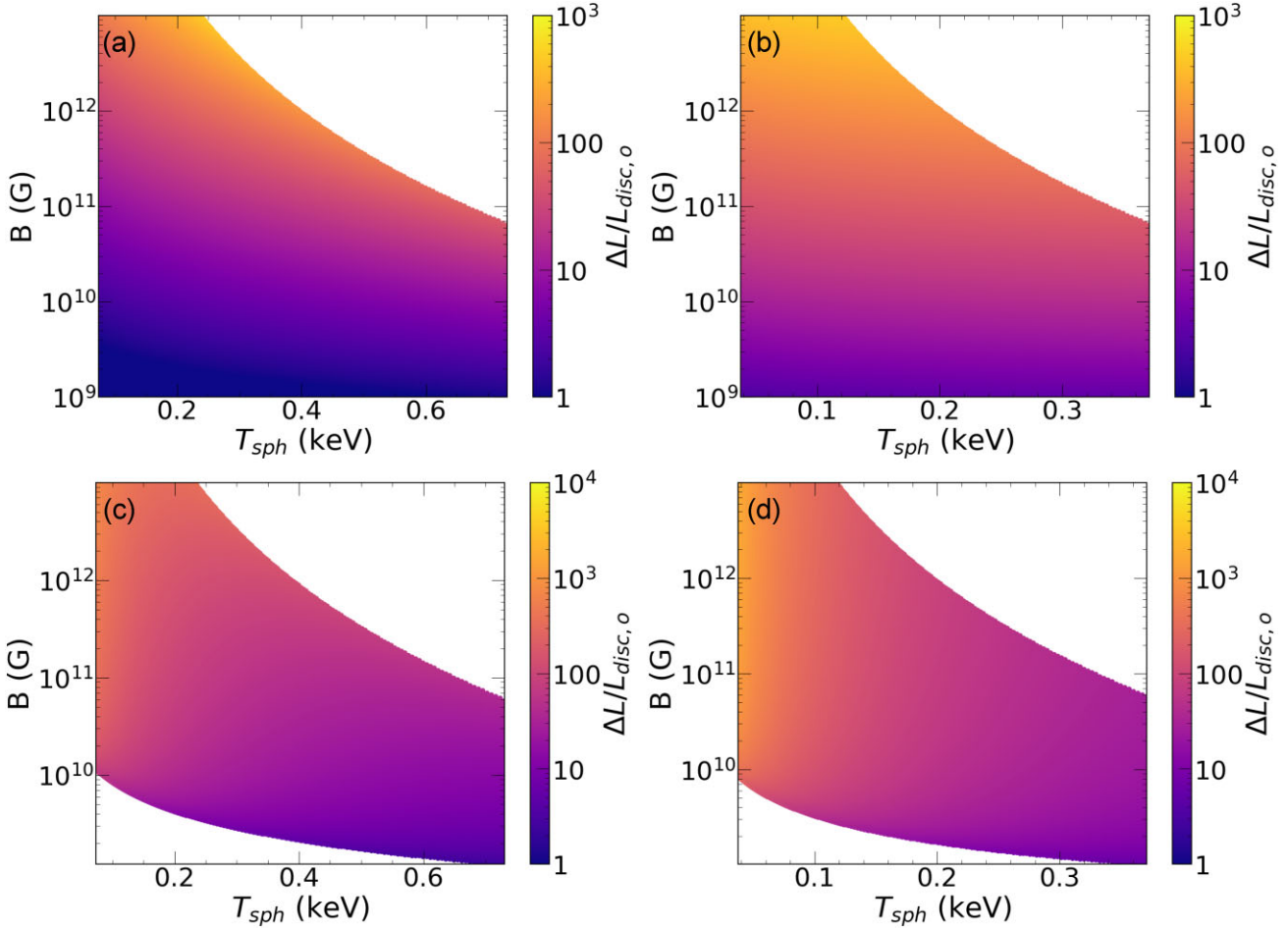


Figure 7. Plots showing the exact solutions for $\Delta L/L_{\text{disc},o}$ on \dot{m}_0 , parametrized here by T_{sph} assuming $b = 0.5$. Panels A & B should be compared to Panels B of Figs 1 and 2 whilst Panels C & D should be compared to Panels B of Figs 3 and 4.

corresponding to a larger advected mass fraction and a smaller R_m for a given dipole field strength. For a fixed inclination angle where we can see into the wind-cone, a larger \dot{m}_0 would imply the source should be brighter due to increased collimation, whilst a smaller \dot{m}_0 – where R_m is larger and can approach R_{co} – should be fainter. Thus, propeller states should be driven mostly by changes in \dot{m}_0 rather than spin-up, we would naturally expect to see ULXs lose their hard component when they are in their faintest states. This is not what is observed in the ULXs we have explored in this paper, where they appear bright (although not as bright as their peak observed luminosity, cf Gúrpile et al. 2021a). This picture becomes more complicated when precession is involved as the brightness and spectral shape are also dependent on phase (Abolmasov, Karpov & Kotani 2009; Middleton et al. 2015a; Narayan, Sałdowski & Soria 2017), implying that propeller transitions could occur without a preferred spectral shape and brightness; exploring this requires monitoring at soft to hard energies.

An alternative possibility to explain changes in the spectra and brightness of the ULXs in this paper is that we are not observing a propeller state but instead long duration dips as material – likely entrained in a wind – passes across our line-of-sight (e.g. Stobbart, Roberts & Warwick 2004; D’Ai et al. 2021; Alston et al. 2021; Gúrpile et al. 2021b, which then obscures the hard component of the spectrum. Although we do not detect obvious dips within the light curves of the putative propeller observations we have analysed,

further distinguishing between these scenarios is beyond the scope of this current work.

There are a number of caveats to this work. In the absence of a radial beaming profile, we have assumed that collimation (determining the value of b in equations 2 & 4) affects the emission equally between R_{sph} and R_m and from within R_m . In reality this is unlikely to be strictly true although becomes increasingly the case as the dipole field strength weakens or as the accretion rate increases. We also do not consider the probable mass loss between R_m and R_{ns} driven by the intrinsically super-Eddington flux from the column or as a result of the mass rate being fed onto the neutron star at larger rates than can be accommodated by the magnetic field (although this may be multipolar in nature and considerably stronger than the dipole: Israel et al. 2017a; Tsygankov et al. 2017; Middleton et al. 2019a; Brice et al. 2021; Kong et al. 2022). If mass losses from the magnetosphere, then the ratio of $\Delta L/L_{\text{disc},o}$ will be smaller for a given dipole field strength, allowing higher dipole field solutions; this remains an open question. In order to remove the beaming factor from our equations, we assumed $\frac{\xi}{b} \ln\left(\frac{R_{\text{sph}}}{R_m}\right) \gg 1$. This is only strictly correct for small ϵ_w , significant beaming (small b) or R_{sph} several factors larger than R_m , where this breaks down (when the beaming is not strong, which will occur as R_m tends to R_{sph}). Our estimate for the relative change in luminosity in Figs 1–4 will be an overestimate. In Fig. 7, we plot the exact solution for magnetic dipole field strength versus T_{sph} versus $\Delta L/L_{\text{disc},o}$ for the limiting

case of very mild beaming with $b = 0.5$ (corresponding to a scale height of only around unity). As can be seen by comparing to panel B of Figs 1–4, the greatest impact occurs where advection of energy is included, permitting smaller values of $\Delta L/L_{\text{disc},o}$ to be reached for a given dipole field strength, as expected. The impact at low ϵ_{wind} and without advection is minimal, which does not affect the constraints we have placed on the dipole field strength in NGC 1313 X-1 (modulo the caveats already discussed).

In future, we hope to build on this initial work by modelling the complete ULX spectrum as it transits into the propeller phase, incorporating the anisotropy of the disc and the key temperatures of the various components (Poutanen et al. 2007; Mushtukov et al. 2017).

ACKNOWLEDGEMENTS

The authors thank the anonymous referee for their useful suggestions. MM and AG acknowledge support via Science and Technologies Facilities Council (STFC) Consolidated grant (ST/V001000/1). The authors thank Hugh Dickinson for useful advice.

DATA AVAILABILITY

Data can be made accessible upon request.

REFERENCES

- Abolmasov P., Karpov S., Kotani T., 2009, *PASJ*, 61, 213
 Alston W. N. et al., 2021, *MNRAS*, 505, 3722
 Bachetti M. et al., 2014, *Nature*, 514, 202
 Bachetti M. et al., 2020, *ApJ*, 891, 44
 Bellm E. C. et al., 2014, *ApJ*, 792, 108
 Brice N., Zane S., Turolla R., Wu K., 2021, *MNRAS*, 504, 701
 Brightman M. et al., 2016, *ApJ*, 816, 60
 Brightman M. et al., 2018, *Nat. Astron.*, 2, 312
 Brightman M. et al., 2019a, *ApJ*, 873, 115
 Brightman M. et al., 2019b, *ApJ*, 873, 115
 Carpano S., Haberl F., Maitra C., Vasilopoulos G., 2018, *MNRAS*, 476, L45
 Chashkina A., Lipunova G., Abolmasov P., Poutanen J., 2019, *A&A*, 626, A18
 Cui W., 1997, *ApJ*, 482, L163
 D’À A. et al., 2021, *MNRAS*, 507, 5567
 Dai H. L., Li X. D., 2006, *A&A*, 451, 581
 Dauser T., Middleton M., Wilms J., 2017, *MNRAS*, 466, 2236
 Earnshaw H. P., Roberts T. P., Middleton M. J., Walton D. J., Mateos S., 2019, *MNRAS*, 483, 5554
 Earnshaw H. P., Roberts T. P., Sathyaprakash R., 2018, *MNRAS*, 476, 4272
 Erkut M. H., 2019, *ApJ*, 873, 105
 Fragos T., Lehmer B. D., Naoz S., Zezas A., Basu-Zych A., 2013, *ApJ*, 776, L31
 Fuerst F. et al., 2021, *A&A*, 651, A75
 Fürst F. et al., 2014, *ApJ*, 780, 133
 Fürst F. et al., 2016, *ApJ*, 831, L14
 Geppert U., Urpin V., 1994, *MNRAS*, 271, 490
 Gúrpide A., Godet O., Koliopanos F., Webb N., Olive J. F., 2021a, *A&A*, 649, A104
 Gúrpide A., Godet O., Vasilopoulos G., Webb N. A., Olive J.-F., 2021b, *A&A*, 654, A10
 Israel G. L. et al., 2017a, *Science*, 355, 817
 Israel G. L. et al., 2017b, *Science*, 355, 817
 Israel G. L. et al., 2017c, *MNRAS*, 466, L48
 Jiang Y.-F., Stone J. M., Davis S. W., 2014, *ApJ*, 796, 106
 Jiang Y.-F., Stone J. M., Davis S. W., 2019, *ApJ*, 880, 67
 Khan N., Middleton M. J., Wiktorowicz G., Dauser T., Roberts T. P., Wilms J., 2022, *MNRAS*, 509, 2493
 King A. R., 2009, *MNRAS*, 393, L41
 King A., Lasota J.-P., 2020, *MNRAS*, 494, 3611
 King A., Lasota J.-P., Kluźniak W., 2017, *MNRAS*, 468, L59
 Koliopanos F., Vasilopoulos G., Buchner J., Maitra C., Haberl F., 2019, *A&A*, 621, A118
 Koliopanos F., Vasilopoulos G., Godet O., Bachetti M., Webb N. A., Barret D., 2017, *A&A*, 608, A47
 Kong L.-D. et al., 2022, *ApJ*, 933, L3
 Kosec P. et al., 2021, *MNRAS*, 508, 3569
 Kosec P., Pinto C., Walton D. J., Fabian A. C., Bachetti M., Brightman M., Fürst F., Grefenstette B. W., 2018, *MNRAS*, 479, 3978
 Kovelakos K., Fragos T., Schaerer D., Mesinger A., 2022, *A&A*, 665, A28
 Kuranov A. G., Postnov K. A., Yungelson L. R., 2020, *Astronomy Letters*, 46, 658
 Marlowe H. et al., 2014, *MNRAS*, 444, 642
 Middleton M. J. et al., 2018, *MNRAS*, 475, 154
 Middleton M. J. et al., 2021, *MNRAS*, 506, 1045
 Middleton M. J., Brightman M., Pintore F., Bachetti M., Fabian A. C., Fürst F., Walton D. J., 2019a, *MNRAS*, 486, 2
 Middleton M. J., Fragile P. C., Ingram A., Roberts T. P., 2019b, *MNRAS*, 489, 282
 Middleton M. J., Heil L., Pintore F., Walton D. J., Roberts T. P., 2015a, *MNRAS*, 447, 3243
 Middleton M. J., Higginbottom N., Knigge C., Khan N., Wiktorowicz G., 2022, *MNRAS*, 509, 1119
 Middleton M. J., King A., 2016, *MNRAS*, 462, L71
 Middleton M. J., King A., 2017, *MNRAS*, 470, L69
 Middleton M. J., Walton D. J., Fabian A., Roberts T. P., Heil L., Pinto C., Anderson G., Sutton A., 2015b, *MNRAS*, 454, 3134
 Middleton M. J., Walton D. J., Roberts T. P., Heil L., 2014, *MNRAS*, 438, L51
 Mushtukov A. A., Portegies Zwart S., Tsygankov S. S., Nagirner D. I., Poutanen J., 2021, *MNRAS*, 501, 2424
 Mushtukov A. A., Suleimanov V. F., Tsygankov S. S., Ingram A., 2017, *MNRAS*, 467, 1202
 Mushtukov A. A., Suleimanov V. F., Tsygankov S. S., Poutanen J., 2015, *MNRAS*, 454, 2539
 Narayan R., Sałdowski A., Soria R., 2017, *MNRAS*, 469, 2997
 Pasham D. R., Strohmayer T. E., 2013, *ApJ*, 774, L16
 Pinto C. et al., 2017, *MNRAS*, 468, 2865
 Pinto C. et al., 2020a, *MNRAS*, 492, 4646
 Pinto C. et al., 2020b, *MNRAS*, 492, 4646
 Pinto C., Middleton M. J., Fabian A. C., 2016, *Nature*, 533, 64
 Pintore F., Zampieri L., Stella L., Wolter A., Mereghetti S., Israel G. L., 2017, *ApJ*, 836, 113
 Poutanen J., Lipunova G., Fabrika S., Butkevich A. G., Abolmasov P., 2007, *MNRAS*, 377, 1187
 Rodríguez Castillo G. A. et al., 2020, *ApJ*, 895, 60
 Sathyaprakash R. et al., 2019, *MNRAS*, 488, L35
 Shakura N. I., Sunyaev R. A., 1973, *A&A*, 500, 33
 Song X., Walton D. J., Lansbury G. B., Evans P. A., Fabian A. C., Earnshaw H., Roberts T. P., 2020, *MNRAS*, 491, 1260
 Stobbart A. M., Roberts T. P., Warwick R. S., 2004, *MNRAS*, 351, 1063
 Tsygankov S. S., Doroshenko V., Lutovinov A. A., Mushtukov A. A., Poutanen J., 2017, *A&A*, 605, A39
 Tsygankov S. S., Lutovinov A. A., Doroshenko V., Mushtukov A. A., Suleimanov V., Poutanen J., 2016b, *A&A*, 593, A16
 Tsygankov S. S., Mushtukov A. A., Suleimanov V. F., Poutanen J., 2016a, *MNRAS*, 457, 1101
 Tully R. B., Courtois H. M., Sorce J. G., 2016, *AJ*, 152, 50
 Urquhart R. T. et al., 2022, *MNRAS*, 511, 4528
 Vasilopoulos G., Petropoulou M., Koliopanos F., Ray P. S., Bailyn C. B., Haberl F., Gendreau K., 2019, *MNRAS*, 488, 5225
 Vasilopoulos G., 2021, *ApJ*, 909, 50
 Verner D. A., Yakovlev D. G., 1995, *A&AS*, 109, 125

Verner D. A., Yakovlev D. G., Band I. M., Trzhaskovskaya M. B., 1993, *At. Data Nucl. Data Tables*, 55, 233
Walton D. J. et al., 2016, *ApJ*, 826, L26
Walton D. J. et al., 2017, *ApJ*, 839, 105
Walton D. J. et al., 2018a, *MNRAS*, 473, 4360
Walton D. J. et al., 2018b, *ApJ*, 856, 128
Walton D. J. et al., 2018c, *ApJ*, 857, L3
Walton D. J. et al., 2020, *MNRAS*, 494, 6012

Wiktorowicz G., Lasota J.-P., Middleton M., Belczynski K., 2019, *ApJ*, 875, 53
Wilms J., Allen A., McCray R., 2000, *ApJ*, 542, 914

This paper has been typeset from a $\text{\TeX}/\text{\LaTeX}$ file prepared by the author.